Biophysical Journal
Article

Biophysical Society

Structural Basis of Protein Kinase Cα Regulation by the C-Terminal Tail

Yuan Yang,[1] Chang Shu,[1] Pingwei Li,[1] and Tatyana I. Igumenova[1,*]
[1]Department of Biochemistry and Biophysics, Texas A&M University, College Station, Texas

ABSTRACT Protein kinase C (PKC) isoenzymes are multi-modular proteins activated at the membrane surface to regulate signal transduction processes. When activated by second messengers, PKC undergoes a drastic conformational and spatial transition from the inactive cytosolic state to the activated membrane-bound state. The complete structure of either state of PKC remains elusive. We demonstrate, using NMR spectroscopy, that the isolated Ca^{2+}-sensing membrane-binding C2 domain of the conventional PKCα interacts with a conserved hydrophobic motif of the kinase C-terminal region, and we report a structural model of the complex. Our data suggest that the C-terminal region plays a dual role in regulating the PKC activity: activating, through sensitization of PKC to intracellular Ca^{2+} oscillations; and auto-inhibitory, through its interaction with a conserved positively charged region of the C2 domain.

INTRODUCTION

Protein kinase C (PKC) isoenzymes regulate numerous cellular processes, such as gene expression (1,2), migration (3), proliferation (4) and apoptosis (5), through phosphorylation of their target proteins. Since their discovery as receptors for tumor-promoting phorbol esters (6), PKCs have been the subject of numerous biochemical and genetic studies that produced a wealth of information about their biological function. The central role of PKCs in signal transduction pathways that control vital cellular processes translates directly into their role in human health. The tumor-suppressing role of PKCs in cancer (7) and their involvement in progression of cardiovascular (8,9) and neurodegenerative (10) diseases underscore the need to understand the molecular basis of PKC regulation. Biophysical and structural studies of PKC (11) have provided valuable information on the conformational rearrangement of these enzymes during the activation process (12,13). The work reported here provides an atomic-level insight into auto-inhibition and sensitization of a conventional PKC to intra-cellular Ca^{2+} oscillations.

Conventional PKC isoenzymes (α, βI/II, and γ) are activated by two second messengers, Ca^{2+} and diacylglycerol (DAG). This process involves a conformational transition from an inactive cytosolic state to an active membrane-associated state. The inactive form is auto-inhibited through the interaction of the N-terminal pseudosubstrate region with the active site of the C-terminal kinase domain (14,15) (Fig. 1 *a*). The membrane recruitment is mediated by the tandem conserved region 1 (C1A and C1B) and the conserved region 2 (C2) domains (16). C1 domains interact with the membrane-embedded diacylglycerol, which is generated in the upstream signaling event. C2 is a Ca^{2+}-sensing domain that associates with anionic phospholipids, but only in response to binding Ca^{2+} ions. Ca^{2+} plays a dual role (17): it makes the loop region of C2, which mediates membrane interactions, more electropositive, and it directly coordinates lipid headgroups. Disruption of the ability of C2 to bind Ca^{2+} through mutagenesis results in the loss of the membrane-binding function and activation of PKC (18). The membrane-binding event relieves the PKC auto-inhibition by expelling the pseudo-substrate region from the active site and thereby enables PKC to phosphorylate its targets.

The spatiotemporal activation sequence is not well understood at either the domain or the atomic level. Specifically, the following questions remain: what is the structure of the latent form of the enzyme? What is the nature of inter-domain interactions? What serves as a trigger for intra-molecular rearrangement that enables the pseudo-substrate release?

There is accumulating evidence that the C-terminal variable-5 (V5) domain of PKC makes an important

Submitted July 28, 2017, and accepted for publication December 21, 2017.
*Correspondence: tigumenova@tamu.edu
Editor: Jeff Peng.
https://doi.org/10.1016/j.bpj.2017.12.030

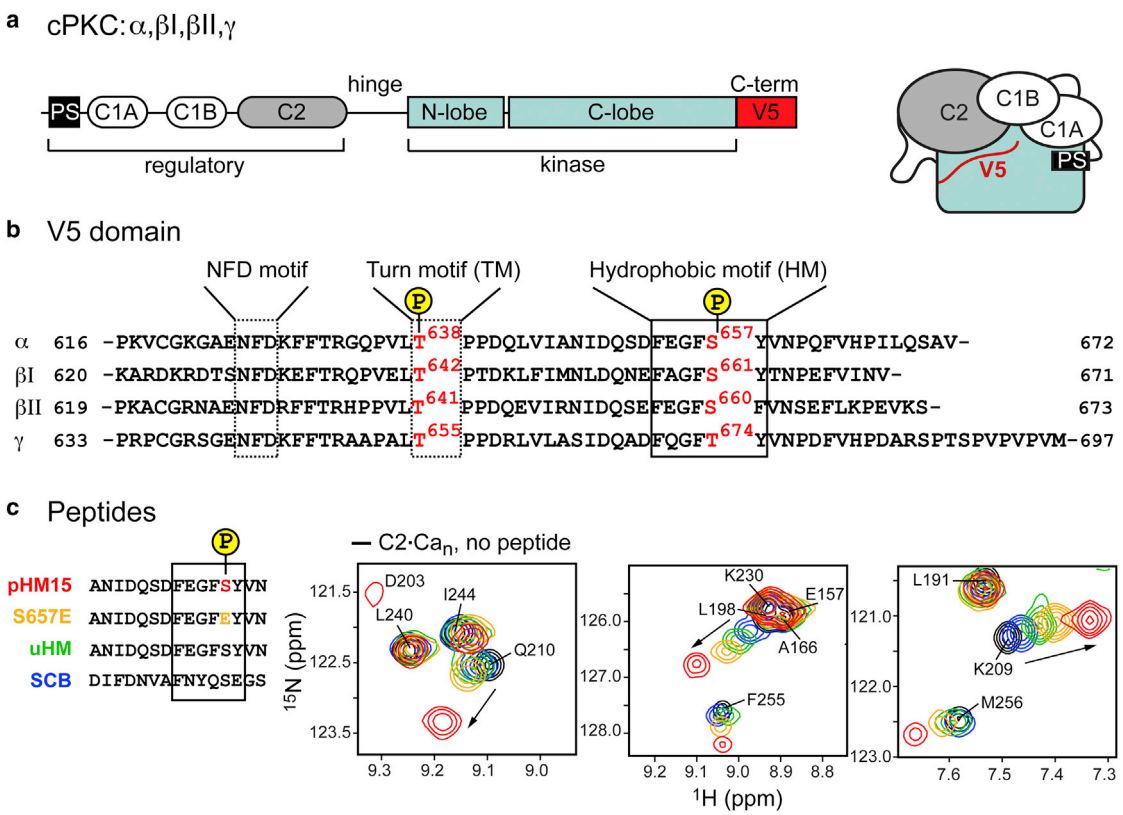

FIGURE 1 Host protein context and interactions between C2 and V5 domains. (*a*) Domain sub-structure of conventional PKC isoenzymes and schematic representation of the inactive form. The Ca^{2+}-sensing C2 and C-terminal V5 domains are shown in gray and red, respectively; PS is a pseudo-substrate region. (*b*) Sequence alignment of C-terminal V5 domains from conventional PKCs. The boxes indicate three conserved motifs, two of which, the HM and the TM, are phosphorylated during enzyme maturation. (*c*) Expansions of ^{15}N-^{1}H HSQC spectra of Ca^{2+}-bound C2 domain ($C2{\cdot}Ca_n$, n = 2,3), in the absence (*black*) and presence of four V5-derived peptides: pHM15, S657E, uHM, and SCB. The changes in crosspeak positions indicate the changes in electronic environment of the backbone N-H groups of C2 due to binding. To see this figure in color, go online.

contribution to maintaining the inactive conformation of PKC isoforms: its mutagenesis and/or deletion resulted in the increased sensitivity of the enzyme to C1 agonists, indicating that inactive conformation is destabilized and the enzyme adopts a more "open" state (19–21). The C-terminal tail is the most variable region of PKCs. It is intrinsically disordered in the isolated form (22) and has a high degree of static and/or dynamic disorder in the crystal structures of the catalytic domains of PKC (23–32). The three conserved regions of V5 are the NFD motif, the turn motif (TM), and the hydrophobic motif (HM) (Fig. 1 *b*). Phosphorylation of the HM and the TM are among the three ordered phosphorylation events required for newly synthesized PKC to become mature and catalytically competent (33,34). V5 plays a role in several processes that regulate the PKC activity, such as Ca^{2+} sensitivity (35), interactions with scaffolding proteins (36,37), and downregulation via interactions with Pin1 (38).

Although the essential role of V5 in maintaining the inactive conformation of PKC is evident, the identity of its intra-molecular interaction partner(s) in PKC is less certain. A partial crystal structure of PKCβII has led to the "C1B clamp" model, in which V5 contributes to auto-inhibition through the interaction of its NFD motif region with the C1B domain (12). A subsequent analysis of the same structure, combined with molecular docking and functional studies, pointed to the involvement of the C2 domain in the auto-inhibitory interaction with the kinase domain and V5 (21). Membrane translocation studies of another Ca^{2+}-dependent PKC isoform, PKCα, suggested that a putative intra-molecular interaction between C2 and V5 plays an important role in determining the sensitivity of the enzyme to diacylglycerol (19).

In this work, we provide, to our knowledge, the first direct experimental evidence for the interaction between the isolated Ca^{2+}-sensing C2 domain of PKCα and its C-terminal V5 domain. We demonstrate that this interaction depends on the phosphorylation state of the hydrophobic motif and is enhanced by Ca^{2+}. The structural model of the complex between the C2 domain and the HM reveals atomic-level details about the domain interface and suggests a possible mechanism for how the C-terminal tail regulates the activity of PKC.

MATERIALS AND METHODS

Protein and peptide preparation for NMR experiments

C2 domain of PKCα from *Rattus norvegicus* (residues 155–293) was expressed in *Escherichia coli* and purified as previously described (39). Uniformly ^{15}N- ([U-^{15}N]) and ^{13}C, ^{15}N-enriched ([U-^{13}C, ^{15}N]) C2 were prepared using (^{15}N, 99%) ammonium chloride and (6-^{13}C, 99%) glucose as the sole nitrogen and carbon sources, respectively. C2 samples were decalcified by incubation with 0.1 mM EDTA, followed by extensive buffer exchange into an EDTA- and Ca^{2+}-free buffer. All buffer solutions were decalcified by passing through Chelex resin (Sigma-Aldrich, St. Louis, MO). For NMR-monitored binding experiments, the final buffer composition was 20 or 10 mM MES at pH 6.0, 8% (v/v) D_2O, and 0.02% (w/v) NaN_3. The peptides were purchased from either GenScript or Eton Bioscience. Crude peptide mixtures were purified on a C18 column using high-performance liquid chromatography (HPLC). Peptide concentration was determined from the absorbance at 280 or 205 nm; additional concentration measurements were carried out for phosphorylated peptides using the phosphate assay (40). The molecular weight and purity of the peptides after HPLC purification were verified using matrix-assisted-laser-desorption-time-of-flight mass spectrometry. The peptide stock solutions were prepared in HPLC-grade water and adjusted to pH 6.0 with ammonium hydroxide.

Insect cell expression and purification of PKCα

pBiEx1 plasmid carrying the mCer-hPKCα-mCit-FLAG gene was a generous gift from Dr. Sivaraj Sivaramakrishnan (University of Minnesota). mCer and mCit encode mCerulean and mCitrine fluorescent proteins, which form a Förster resonance energy transfer (FRET) donor-acceptor pair. Human and rat PKCα have identical amino acid sequences of their V5 domains and a single amino acid difference in the C2 domain at position 169 (Ala in human, Thr in rat), which is not part of any functional region. For recombinant PKCα expression, the mCer-hPKCα-mCit-FLAG sequence was sub-cloned into pAcGHLT-C (BD Biosciences, Franklin Lakes, NJ) and pBac-1 (EMD Millipore, Burlington, MA) vectors. Either pAcGHLT-C or pBac-1 plasmid was co-transfected with ProGreen linearized baculovirus DNA (AB Vector) into Sf9 cells to generate recombinant baculovirus. The Sf9 cells at a density of 2.5×10^6/mL were infected with recombinant baculovirus of high titer in a serum-free medium (Expression Systems, Davis, CA).

The cells were cultured in suspension at 27°C and harvested after 60 h. The cell pellets were resuspended in a lysis buffer containing 50 mM Tris-HCl at pH 7.5, 1 mM EGTA, 1 mM EDTA, 3 mM $MgCl_2$, 150 mM NaCl, Halt protease inhibitor cocktail (Thermo Scientific, Waltham, MA), 1 mM phenylmethylsulfonyl fluoride, and 1% Triton X-100. The cell suspension was gently mixed on a nutator at 4°C for 30 min to complete the lysis. The mCer-hPKCα-mCit-FLAG was purified using anti-FLAG M2 affinity gel (Sigma-Aldrich). The eluted protein was further purified from low-molecular-weight contaminants and buffer-exchanged on a 50-kDa MWCO spin concentrator (Corning, Corning, NY). The kinase activity was assayed with the PepTag non-radioactive PKC assay kit (Promega, Madison, WI) according to the manufacturer's instructions. The total protein quantity per assay was 20 ng in the reaction volume of 25 μL. The protein concentration was determined using the extinction coefficient of mCit, $\varepsilon(516\text{ nm}) = 77{,}000\ M^{-1}\ cm^{-1}$ (41).

Activity assays in the presence of 1 mM 10-residue pHM peptide were carried out using 20 ng of mCer-hPKCα-mCit-FLAG in the reaction buffer containing 20 mM HEPES (pH 7.4), 1 mM DTT, 3.5 mM $MgCl_2$, 1 mM ATP, and appropriate PKC activators where applicable. The concentrations of activators were 1 mM $CaCl_2$, 0.5 μM phorbol 12,13-dibutyrate (PDBu; Sigma-Aldrich), and 1 mM large unilamellar vesicles (LUVs). LUVs were composed of 1-palmitoyl-2-oleoyl-*sn*-glycero-3-phosphocholine (POPC), 1-palmitoyl-2-oleoyl-*sn*-glycero-3-phospho-L-serine (POPS), and 1,2-dimyristoyl-*sn*-glycerol (DAG), all from Avanti Polar Lipids (Alabaster, AL). The molar ratio of the components was POPC/POPS/DAG 65:30:5. All reactions were carried out at 30°C for 30 min and quenched for 10 min at 95°C. The amount of phosphorylated peptide was quantified using a photon-counting spectrofluorometer (ISS, Champaign, IL). The experiments were carried out in triplicate, and repeated twice for two independent preparations of PKCα in the activator-free assays. The results are reported as the mean ± SD.

Steady-state fluorescence spectroscopy

The steady-state fluorescence emission spectra of purified mCer-hPKCα-mCit-FLAG proteins were recorded at 25°C on a photon-counting spectrofluorimeter (ISS) using an excitation wavelength of 430 nm and a detection range of 450–650 nm. The excitation and emission slit widths were set to 8 nm. The cuvettes were coated with Sigmacote (Sigma-Aldrich) to minimize protein adsorption on the walls. Protein samples with concentrations ranging from 7 to 50 nM were prepared in a decalcified buffer containing 20 mM HEPES at pH 7.4, 100 mM KCl, and 5 mM β-mercaptoethanol. FRET efficiency was calculated as the ratio of peak intensities corresponding to the emission maxima of mCit at 525 nm and mCer at 475 nm. To obtain the reference fluorescence spectra of mCit and mCer in the absence of intramolecular interactions, wild-type mCer-hPKCα-mCit-FLAG was subjected to limited proteolysis with endoproteinase Lys-C (Thermo Scientific, Waltham, MA) that leaves the fluorescent proteins intact. The reaction was carried out at 30°C at a protein/Lys-C ratio of 20:1 (w/w). The fluorescence spectrum was acquired 30 min after initiating the reaction. The completeness of the cleavage reaction was verified using sodium dodecyl sulfate polyacrylamide-gel electrophoresis.

NMR-detected binding of ligands to C2

The ligand-binding experiments were conducted by adding aliquots of concentrated pHM15 (or Ca^{2+}) stock solutions to apo and Ca^{2+}-bound (or apo and pHM15-bound) [U-^{15}N] C2 domain. The protein concentration in the NMR samples ranged from 80 to 100 μM. Ca^{2+} stock solutions were prepared from 1.0 M standard calcium chloride solution (Fluka Analytical, St. Gallen, Switzerland). For each ligand concentration, ^{15}N-^{1}H heteronuclear single-quantum correlation (HSQC) spectra were collected at 25°C on Varian INOVA spectrometers operating at Larmor ^{1}H frequencies of 500 or 600 MHz. For the chemical shift perturbation (CSP) and binding-curve analysis, the residue-specific chemical-shift change between any given pair of C2 states was calculated using the equation

$$\Delta = \sqrt{(\Delta\delta_H)^2 + (0.152 \times \Delta\delta_N)^2}, \quad (1)$$

where $\Delta\delta_H$ and $\Delta\delta_N$ are the residue-specific differences in the ^{1}H and ^{15}N chemical shifts, respectively. The binding curves were constructed by plotting Δ against the total ligand concentration. The dissociation constant, K_d, for the pHM15 binding to C2 was determined by fitting the binding curves with the single-site equation,

$$\Delta = (\Delta_{max}/2P_0)\left[P_0 + L_0 + K_d - \sqrt{(P_0 + L_0 + K_d)^2 - 4P_0L_0}\right], \quad (2)$$

where Δ_{max}, P_0, and L_0 are the chemical-shift change at complete saturation, total protein concentration, and total ligand concentration, respectively. The apparent dissociation constants, $K_{d,app}$, for Ca^{2+} binding to

C2 were acquired by fitting the binding curves with the modified Hill equation (42) to account for the moderate cooperativity of Ca^{2+} binding:

$$\Delta = \Delta_{max}\frac{\left(L_0 - \left(P_0 + L_0 + K_{d,app} - \sqrt{\left(P_0 + L_0 + K_{d,app}\right)^2 - 4P_0L_0}\right)\Big/2\right)^{n_{app}}}{K_{d,app}^{n_{app}} + \left(L_0 - \left(P_0 + L_0 + K_{d,app} - \sqrt{\left(P_0 + L_0 + K_{d,app}\right)^2 - 4P_0L_0}\right)\Big/2\right)^{n_{app}}}, \quad (3)$$

where n_{app} is the Hill coefficient that reports on the apparent cooperativity (43) of Ca^{2+} binding. More details on the binding data analysis, including the criteria for residue selection and all individual binding curves, are given in the Supporting Material, Sections 3–5.

NMR experiments for structure validation, resonance assignment, and structural restraints

We used lanthanide (Ln^{3+})-induced pseudocontact shift (PCS) values to assess the structure of the pHM-complexed C2. The peptide pHM corresponds to a highly soluble 10 amino acid version of the hydrophobic motif, Ac-DQSDFEGFpSY-NH_2. The complexes of [U-^{15}N,^{13}C] C2 with Ln^{3+} (Ln = La, Tb, and Tm) were prepared by combining equimolar amounts of C2 and $LnCl_3$ (Sigma Aldrich) dissolved in HPLC-grade water. In the pHM-containing sample, the concentration of pHM was 600 μM and the concentration of the C2•Ln^{3+} complexes ranged from 40 to 60 μM. ^{15}N-^{1}H HSQC spectra were collected at 25°C on Avance III spectrometers (Bruker Biospin, Billerica, MA) operating at ^{1}H Larmor frequencies of 500 and 600 MHz. The PCS values were determined by subtracting the residue-specific ^{1}H and ^{15}N C2 chemical shifts of La^{3+}-containing diamagnetic complexes from those of Tm^{3+}-and Tb^{3+}-containing paramagnetic complexes. The resonance assignment of diamagnetic C2•La^{3+} spectra was done by comparison with the previously assigned spectrum of single Pb^{2+}-bound C2 (39). The resonance assignment of the paramagnetic C2 spectra was done iteratively as implemented in Numbat (44), using the Pb^{2+}-complexed structure of C2 (Protein Data Bank (PDB): 3TWY).

Two NMR samples, with either C2 or the HM peptide in molar excess, were prepared for structural characterization of the C2•Ca^{2+}•pHM complex. Sample 1 contained 0.89 mM [U-^{13}C, ^{15}N] C2, 2.23 mM $CaCl_2$, and 2 mM pHM. Sample 2 contained 1.47 mM [U-^{13}C, ^{15}N] C2, 3.75 mM $CaCl_2$, and 0.6 mM pHM. The final buffer conditions after preparation of the C2•Ca^{2+}•pHM complex were 6.7 mM MES at pH 6.0, 67 mM KCl, 8% (v/v) D_2O, and 0.02% (w/v) NaN_3. All NMR data were collected at 23°C using Avance III NMR instruments (Bruker Biospin) operating at the ^{1}H Larmor frequencies of 500, 600, and 800 MHz, the latter two equipped with a cryogenically cooled probe. For sample 1, the resonances of backbone ^{1}H, ^{13}C, and ^{15}N atoms of the pHM-complexed C2 were assigned using two-dimensional (2D) ^{15}N-^{1}H HSQC, three-dimensional (3D) HNCO (45), 3D HN(CA)CO (46), and 3D HNCACB (45) experiments. The resonances of side-chain ^{13}C and ^{1}H atoms were assigned using 2D [^{13}C-^{1}H] HSQC, 3D CC(CO)NH (47), 3D H(CCO)NH (48), 3D HCCH-total correlation spectroscopy (TOCSY) (49), 3D HCCH-correlation spectroscopy (COSY) (50), and 3D ^{15}N-TOCSY-HSQC (51) experiments. The resonances of aromatic ^{1}H atoms were assigned with 2D aro-[^{13}C-^{1}H] HSQC and 3D aro-HCCH-TOCSY experiments.

The NOE restraints for calculating the structure of C2 were obtained from the 3D ^{13}C-edited nuclear Overhauser effect spectroscopy (NOESY)-HSQC and ^{15}N-edited NOESY-HSQC experiments (51–53) conducted on sample 1. Inter-molecular C2-pHM NOE restraints were obtained from 2D [F2] ^{15}N, ^{13}C-filtered NOESY, 3D [F1] ^{15}N,^{13}C-filtered NOESY-^{15}N-HSQC, and 3D [F1] ^{15}N, ^{13}C-filtered NOESY-^{13}C-HSQC (54) spectra. The inter-molecular origin of these crosspeaks was verified using 2D [F1] ^{15}N, ^{13}C-filtered NOESY and 2D [F1, F2] ^{15}N,^{13}C-filtered NOESY experiments (55). The ^{1}H atoms of the C2-bound pHM in sample 2 were assigned with 2D [F1, F2] ^{15}N, ^{13}C-filtered TOCSY, and 2D [F1, F2] ^{15}N,^{13}C-filtered NOESY spectra; the latter was used to obtain the NOE restraints for the calculation of the pHM structure. The mixing time for all NOESY experiments was 120 ms. All NMR data were processed using NMRPipe (56). The analysis and all-atom assignments were performed with Sparky (57).

Calculation of NMR structures and assembly of the ternary complex

Automated NOE assignment, calculation of the Ca^{2+}-bound C2 structure in the context of the C2•$Ca^{2+}{}_2$•pHM ternary complex, and its refinement in explicit solvent were carried out using ARIA software (version 2.3) (58). The ^{1}H-^{1}H distance restraints were determined from the volumes of crosspeaks in the 3D NOESY spectra. Hydrogen bonds were identified based on the ^{1}H-^{2}D exchange rates of amide ^{1}H atoms. Dihedral angles were predicted by TALOS+ (59) using a complete set of ^{15}N, ^{13}C′, $^{13}C^{\alpha}$, $^{13}C^{\beta}$, $^{1}H^{\alpha}$, and $^{1}H^{N}$ chemical shifts. Metal coordination restraints in the range 2.1–2.5 Å between the Ca^{2+} ions and the coordinating oxygens of C2 were also included. The refined structural ensemble of the Ca^{2+}-complexed C2 was deposited in the PDB (PDB: 2NCE). The structure of the C2-bound pHM was calculated using 100 NOE restraints obtained from the 2D [F1, F2] ^{15}N,^{13}C-filtered NOESY spectra. After refinement in explicit solvent, the 20 lowest-energy structures were selected for the final NMR ensembles and validated by PROCHECK-NMR (60).

The model of the C2•$Ca^{2+}{}_2$•pHM complex was generated using HADDOCK 2.2 (61,62). To generate initial structures, all combinations of Ca^{2+}-bound C2 and pHM structures were drawn from their respective NMR ensembles. The unambiguous distance restraints consisted of 29 intermolecular NOEs between the ^{1}H atoms of C2 and pHM, and 12 metal ion-oxygen restraints for the two Ca^{2+} ions bound to C2. The ambiguous restraints were based on the extent of ^{1}H and ^{15}N CSPs experienced by the C2 residues as a result of pHM binding. The "active" residues of C2 were defined as those having CSP values at least one standard deviation above the mean and all-atom surface accessibility of >50%, determined using Naccess (63). All pHM peptide residues were treated as "passive."

The calculations generated 6000/400/400 models for the rigid body docking, semi- and fully- flexible simulated annealing, and explicit solvent refinement stages. The final 400 models were subjected to cluster analysis, as described by Daura et al. (64). The HADDOCK scores for all clusters are given in Table S6. The 20 top-scoring structures of the C2•$Ca^{2+}{}_2$•pHM complex were deposited under PDB: 5W4S. Electrostatic potential calculations were conducted using the Adaptive Poisson Boltzmann Solver (65) implemented through the Visual Molecular Dynamics (66) plugin. The PDB-format files were prepared for electrostatics calculations using PDB2PQR (67).

RESULTS

Phosphorylation of the hydrophobic motif enhances its interaction with C2

Previous work on PKCα suggested that its C-terminal tail, specifically, the HM, plays a role in determining the DAG sensitivity of the enzyme. Based on the DAG-stimulated membrane translocation behavior of PKCα variants, Larsson and Stensman (19) hypothesized that the C-terminal V5 domain and C2 may be involved in intra-molecular interaction that renders the enzyme insensitive to DAG.

Our first step was to investigate whether isolated HM interacts with C2 in solution. We designed four synthetic peptides to probe this interaction (Fig. 1 *c*). pHM15 is the phosphorylated HM representing its state in the mature kinase; S657E has the phospho-mimicking glutamic acid in place of the phosphorylated Ser657; unphosphorylated peptide uHM mimics the state of the immature unphosphorylated kinase; and SCB is the scrambled sequence of uHM with the same overall charge and amino acid composition. The peptides were added to the Ca^{2+}-complexed ^{15}N-enriched C2 domain at 20-fold molar excess. Under our experimental conditions, 100 μM C2 and 2.5 mM Ca^{2+}, the protein is partitioned between C2$\cdot Ca_2$ and C2$\cdot Ca_3$ states with fractional populations of ~92 and 8%, respectively (68); we will subsequently refer to the Ca^{2+}-complexed state of C2 as C2$\cdot Ca_n$. We recorded the ^{15}N -^{1}H HSQC spectra of the peptide-containing C2 samples and compared them with the spectrum of the peptide-free C2. All four peptides interact with the C2 domain to a different extent, as indicated by changes in the ^{1}H and ^{15}N chemical shifts of several N-H groups of C2 (Fig. 1 *c*). The concentration of C2, Ca^{2+}, and peptides were identical for all samples. Therefore, the magnitude of CSPs can be used to qualitatively evaluate the affinity of peptide binding to C2: pHM15 > S657E > uHM > SCB. We conclude that the phosphorylation of the HM enhances its interactions with C2.

Synergy between Ca^{2+} and the HM

Ca^{2+} binding to the C2 domain is the first step of the PKC activation process. We used solution NMR to determine the effect of Ca^{2+} on the interactions of the HM with C2. The concentration of pHM15 in the sample containing either [U-^{15}N] apo C2 or C2$\cdot Ca_n$ was varied from zero to 1.5 mM. The ^{15}N-^{1}H HSQC spectra were collected at each concentration of pHM15 and overlaid to identify the C2 residues that experienced CSPs due to interactions with the peptide. For both C2 states, a significant number of C2 residues showed changes in their N-H chemical shifts (Fig. 2, *a* and *b*; see Fig. S1 for full spectra). The majority of C2 crosspeaks follow a smooth trajectory as a result of increasing pHM15 concentration, indicating that the binding process is fast on the NMR chemical-shift timescale irrespective of the state of metal ligation.

We applied CSP analysis to identify the C2 regions affected by the interactions with the HM. CSP values, Δ, were calculated between a pair of C2 states containing no peptide and 1.5 mM pHM15, and plotted against the amino acid sequence of C2 (Fig. 2 *c*). Although the magnitude of chemical-shift changes in the apo C2 (Fig. 2 *c*, *bottom*) is smaller than that for C2$\cdot Ca_n$ (Fig. 2 *c*, *top*), the overall pattern is quite similar. We conclude that Ca^{2+} binding does not significantly change the interaction mode of C2 with HM.

The crystal structure of the Ca^{2+}-bound C2 (69) provides a structural context for interpreting the observed CSPs. We chose this particular structure to show the position of the weak third Ca^{2+} site, whose presence is detectable by NMR at high Ca^{2+} concentrations (Fig. S2) (68). The C2 domain has two major functional regions, the Ca^{2+}- and membrane-binding loops (CMBLs) and the lysine-rich cluster (LRC). CMBL1 and CMBL3 provide oxygen-containing ligands for Ca^{2+} ions that bridge the protein and negatively charged groups of anionic phospholipids. LRC is the interaction site of the C2 domain with a signaling lipid PtdIns(4,5)P_2 (69). The CSP data show that the regions significantly affected by the interactions with the HM include the major functional elements of C2, namely, CMBL1, CMBL3, and the LRC. The C-terminal helix, H3, is also affected, but to a lesser extent. A similar pattern of CSPs was previously observed in NMR studies of PtdIns(4,5)P_2-C2 interactions (70), suggesting that the interaction surface of the C2 domain with HM includes the LRC.

To determine how Ca^{2+} and pHM15 influence each other's affinity for the C2 domain, we conducted a total of four NMR-detected binding experiments, in which we added 1) pHM15 to Ca^{2+}-complexed C2; 2) pHM15 to apo C2; 3) Ca^{2+} to pHM15-complexed C2; and 4) Ca^{2+} to apo C2. To determine the ligand affinities, we constructed binding curves by plotting the residue-specific chemical-shift changes against the total ligand concentration. One special consideration for binding experiment 1 was to ensure that our analysis reflects the binding of pHM15 only and is not affected by the C2 domain picking up additional Ca^{2+} through its normally weak third site. The latter scenario is feasible based on our previous finding that neutralizing the electropositive LRC region through interactions with negatively charged PtdIns(4,5)P_2 resulted in an increase of the C2 affinity to divalent metal ions (70). More details on selection criteria, all binding curves, and other relevant details of data analysis are given in the Supporting Material, Sections 3–5.

The main outcomes of our experiments are illustrated using representative binding curves (Fig. 3) that we selected based on the following criteria: 1) binding curves for a given residue are available for both states; and 2) the residues belong to the major functional elements of C2. Our first

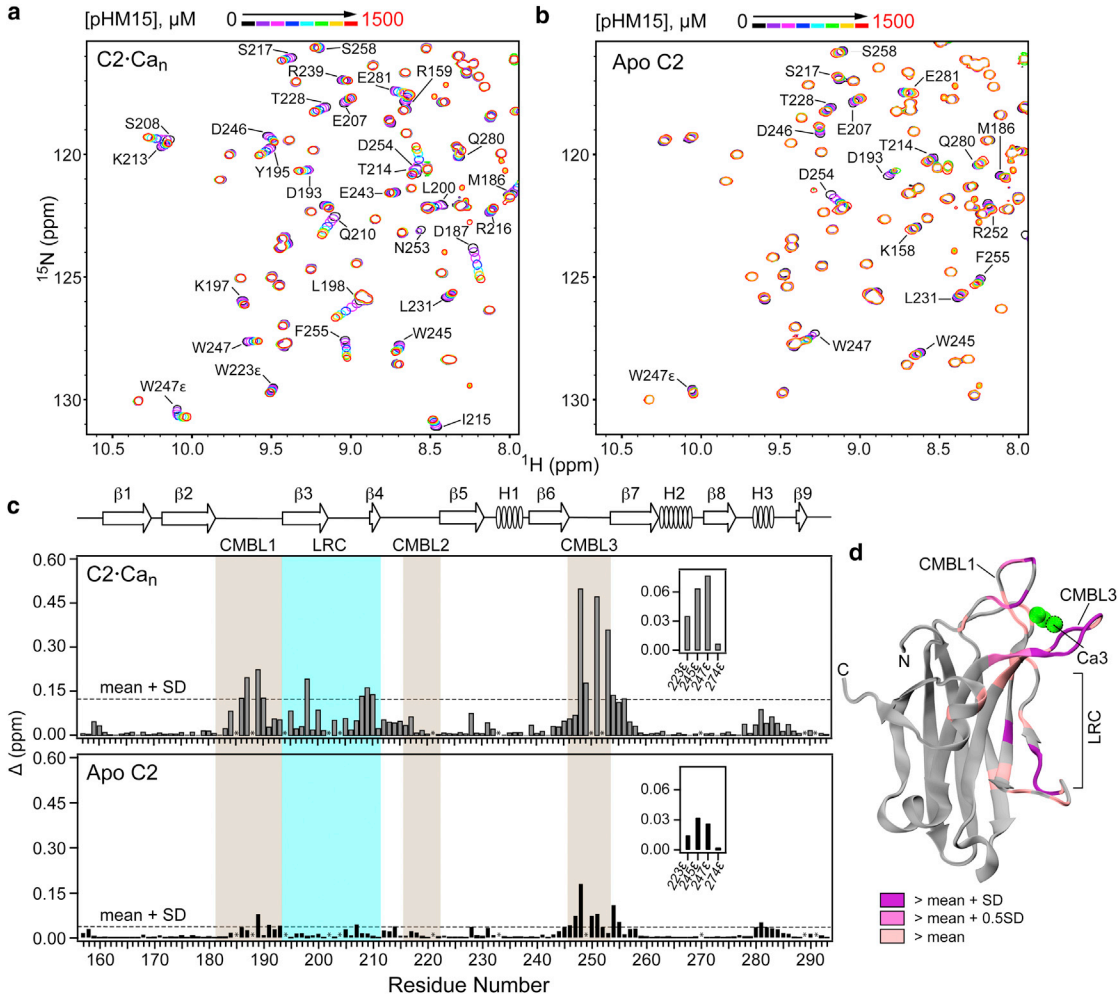

FIGURE 2 The HM interacts with apo and Ca^{2+}-bound C2. (*a* and *b*) Expansions of ^{15}N-^{1}H HSQC spectra of [U-^{15}N] apo C2 (*a*) and C2•Ca$_n$ (*b*), showing the effect of increasing the pHM15 concentration, [pHM15]. The spectra are overlaid and color-coded according to [pHM15]. The N-H groups of C2 whose chemical shift changes as a result of binding are labeled. (*c*) CSPs, Δ, due to pHM15 binding for all spectrally resolved residues of C2•Ca$_n$ (*top*) and apo C2 (*bottom*). Residue-specific Δ values were calculated using spectra with zero and 1.5 mM [pHM15] for C2•Ca$_n$ (*top*) and apo C2 (*bottom*). Asterisks indicate residues that are either prolines or broadened/not spectrally resolved. The insets show CSPs for the indole side-chain amine groups of the four Trp residues. (*d*) Crystal structure of the C2 domain complexed to three Ca^{2+} ions, PDB: 3GPE. The CSPs of the Ca^{2+}-complexed C2 domain due to pHM binding are color-coded and mapped onto the structure. Ca^{2+} ions are shown as green spheres. To see this figure in color, go online.

finding was that Ca^{2+} increases the affinity of C2 for the HM ~2.0-fold, based on the K_d values of 116 ± 5 and 200 ± 5 μM for the Ca^{2+}-bound and apo C2, respectively (Fig. 3 *a*; Figs. S3 and S4). The converse experiments, where we measured the affinity of the C2 domain for Ca^{2+} in the absence and presence of pHM15 (Fig. 3 *b*; Fig. S6) revealed the same pattern: the presence of pHM15 increased the affinity of C2 for Ca^{2+} ~4-fold. The median $K_{d,app}$ value decreased from 393 to 108 μM, whereas the apparent Hill coefficient increased from 1.3 to 1.5. We conclude that there is a clear synergy between Ca^{2+} and pHM15 interactions with C2, as manifested in the mutual enhancement of their respective affinities to the C2 domain.

How do our in vitro affinity measurements relate to the behavior of the full-length PKC? In the full-length enzyme, the HM and C2 reside on the same polypeptide chain. This would favor the formation of the intra-molecular C2-pHM interaction even in the absence of Ca^{2+}. Our binding data suggest that intra-molecular C2-pHM interaction will increase at least fourfold the Ca^{2+} affinity for the inactive PKC compared to that of the isolated C2 domain. The Ca^{2+} sensitivity of PKC increases even further in the presence of acidic phospholipids, ultimately making the membrane binding and subsequent activation possible at low micromolar concentrations of Ca^{2+} (71,72).

Structural characterization of the C2·(Ca^{2+})$_2$·pHM complex

To dissect the structural basis of the interactions between C2 and the HM, we prepared a complex consisting of Ca^{2+}-bound C2 and a 10-residue pHM peptide. pHM binds to

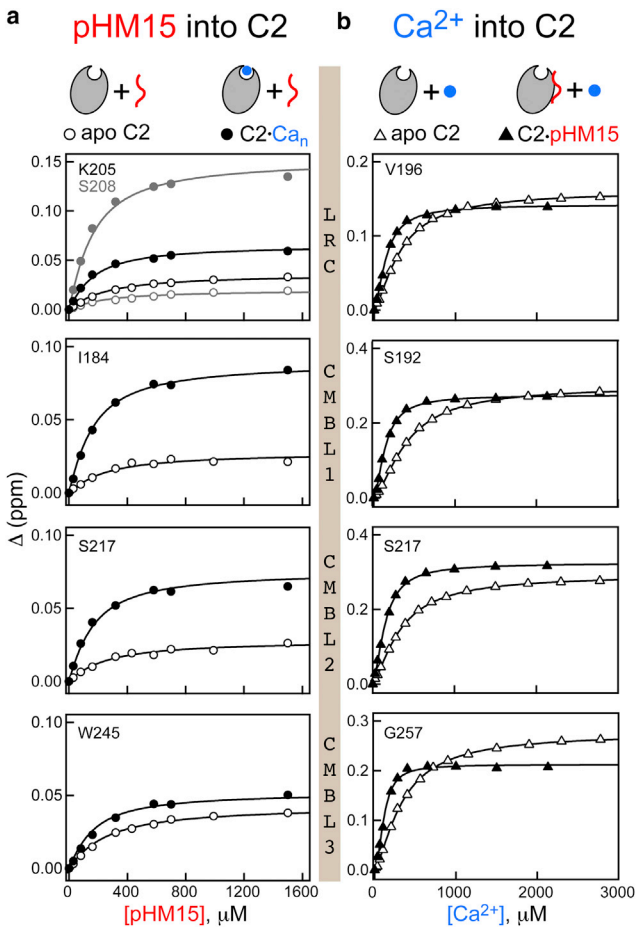

FIGURE 3 Synergistic action of Ca^{2+} and the HM. (*a*) Representative curves for pHM15 binding to apo C2 (*open circles*) and C2•Ca_n (*solid circles*). (*b*) Representative curves for Ca^{2+} binding to apo C2 (*open triangles*) and C2•pHM15 (*solid triangles*). In both cases, the affinity of one ligand is enhanced in the presence of the other. To see this figure in color, go online.

the same C2 site as pHM15 (Fig. S7), but has slightly higher affinity to Ca^{2+}-complexed C2 (K_d of 94 ± 3 μM), and higher solubility than pHM15, which was crucial for the preparation of samples used in structural work. As a first step, we determined the structure of the C2 domain in the context of the complex using NMR spectroscopy. The experimental restraints included NOEs, dihedral angles, hydrogen bonds, and metal ion-oxygen coordination restraints for two Ca^{2+} ions (Table S3). Superposition of the solution NMR ensemble of C2•$(Ca^{2+})_2$ onto the crystal structures of apo (PDB: 3RDJ (39)) and Ca^{2+}-bound C2 (PDB: 1DSY (73)) produced a backbone root mean-square deviation (RMSD) value of 1.1 ± 0.1 Å for both (Fig. 4 *a*).

To establish whether the structures of pHM-free and complexed C2 are similar in solution, we compared the ^{1}H and ^{15}N pseudo-contact shifts (PCSs) that are induced by paramagnetic lanthanides. Lanthanide-induced PCSs are sensitive reporters of protein structure through their dependence on polar coordinates of NMR-active nuclei in the coordinate frame of the magnetic susceptibility tensor, $\Delta\chi$. The C2 domain binds one Ln^{3+} ion with high affinity. The binding site coincides with the high-affinity Pb^{2+} binding site that we previously characterized (39).

We chose two paramagnetic lanthanide metal ions, Tb^{3+} and Tm^{3+}, that have relatively large $\Delta\chi$, but opposite signs of axial and rhombic $\Delta\chi$ components (Fig. 4 *b*). The PCS values were calculated as the difference between the chemical shifts in the paramagnetic and diamagnetic La^{3+} complexes of C2. To ensure that the majority of C2 is in the pHM-bound form, we used samples with a 15-fold molar excess of pHM over C2. For both Tb^{3+} and Tm^{3+}, we observed an excellent correlation between the backbone PCS values of C2 residues—including those that belong to the LRC—in the absence and presence of pHM (Fig. 4 *c*). These results indicate the similarity of the C2 backbone conformation in the pHM-free and -bound forms.

To determine the conformation of pHM in the C2•$(Ca^{2+})_2$•pHM complex, a separate NMR sample was prepared with C2 in molar excess to ensure that ≥90% of pHM was in the C2-complexed form. We obtained the intra-peptide NOEs from the [^{15}N,^{13}C]-filtered 2D ^{1}H-^{1}H NOESY spectrum of the complex. A comparison of the NOESY spectra of the free and C2-bound pHM shows clear signatures of interactions with C2, such as an increase in rotational correlation time and chemical-shift changes due to complex formation (Fig. S8). A total of 99 unambiguous NOEs were used in the pHM structure calculations. The overwhelming majority of those were intra-molecular and sequential, whereas only two were medium-range (Table S2). The NMR ensemble of pHM shows an extended conformation of the peptide, with a backbone RMSD of 2.4 ± 0.6 Å (Fig. S9). This conformation is rather common in protein-peptide complexes: structural analysis of the 103 non-redundant complexes showed that 64% of the peptides bind in extended or coil conformations, whereas only 17.5 and 18.5% have α- and β-strand conformations, respectively (74).

C2•$(Ca^{2+})_2$•pHM complex is stabilized by electrostatic and aromatic interactions

To obtain structural restraints for the C2•$(Ca^{2+})_2$•pHM complex, we conducted isotope-filtered/edited NOESY experiments that produced 29 inter-molecular NOEs between the C2 and pHM. Such a low number of inter-molecular NOEs was expected due to the low affinity of the complex. De novo structure calculation produced a complex in which pHM is bound to the LRC of C2, but with an under-restrained N-terminus. This is because all inter-molecular NOEs are from the aromatic-rich C-terminal part of pHM (Table S4). We therefore opted to use HADDOCK 2.2/CNS 1.3, which uses (among other terms) an inter-molecular electrostatic energy term to score the structures. Inter-molecular NOEs were used as unambiguous restraints, whereas CSPs of the ^{15}N and $^{1}H_N$ of C2 due to pHM binding

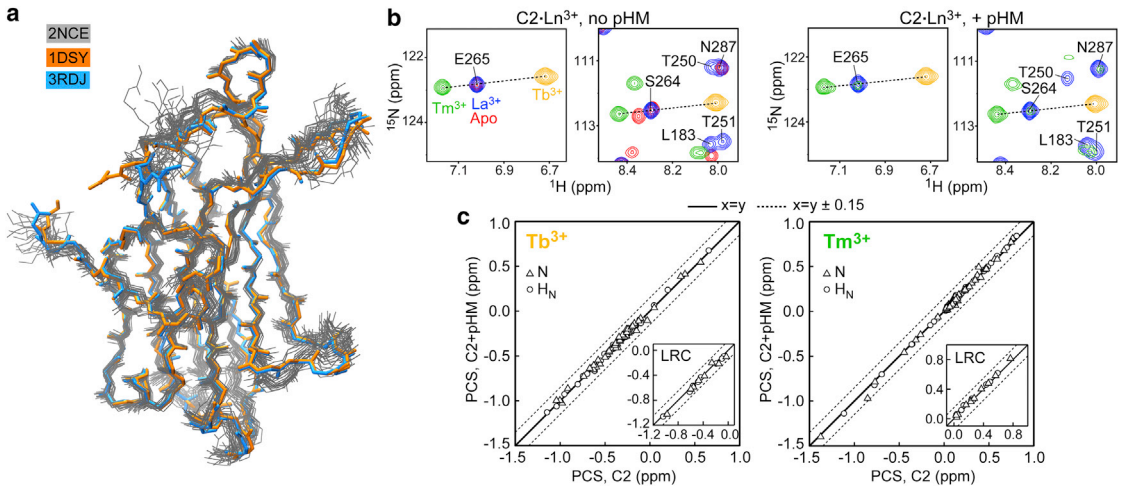

FIGURE 4 (*a*) Backbone superposition of the C2•$(Ca^{2+})_2$ NMR ensemble (PDB: 2NCE, *gray*) in the pHM complex with the crystal structures of the apo (PDB: 3RDJ, *blue*) and Ca^{2+}-complexed C2 (PDB: 1DSY, *orange*). (*b*) Expansions of the ^{15}N-^{1}H HSQC spectra showing Ln^{3+}-induced pseudocontact shifts of C2•Ln^{3+} in the absence and presence of a 15-fold molar excess of pHM. (*c*) The corresponding correlation plot of the PCS values. The inset shows the PCS correlation data for the LRC residues; the LRC is the interaction site of pHM with C2. The solid lines are x = y, whereas dashed lines are x = y ± 0.15; ±0.15 is a typical uncertainty of PCS measurements. To see this figure in color, go online.

were used as ambiguous restraints (Table S4). The NMR ensembles of Ca^{2+}-bound C2 and pHM, both in the context of C2•$(Ca^{2+})_2$•pHM complex, were then used to generate its structural model.

The 400 structures of the C2•$(Ca^{2+})_2$•pHM complex produced during the final refinement step consistently have the pHM interacting with the concave face of C2 that bears the LRC region. The most populated cluster 1 contained 41.5% of the structures and also had the lowest average inter-molecular interaction energy among the six clusters. The 20 top-scoring structures of the C2•$(Ca^{2+})_2$•pHM complex also belong to cluster 1 and form a tight ensemble with a backbone RMSD of 0.41 ± 0.05 Å for the C2 domain and 0.8 ± 0.2 for the pHM (Table S5).

The top-ranking structures of C2•$(Ca^{2+})_2$•pHM illustrate the interaction mode between the HM and the C2 domain (Fig. 5 *a*). pHM binds to the concave face of the C2 domain, and makes contact with two major functional elements, the LRC region and the Ca^{2+}-binding loop CMBL3. The conformation of pHM is extended, with the N-terminus pointing toward the loop between strands β3 and β4 of the LRC and the C-terminus pointing toward CMBL3. The C2-pHM interface is stabilized by electrostatic and aromatic interactions (Table S7). Electrostatic interactions involve salt bridges between the negatively charged side chains of the pHM residues and the positively charged side chains of the C2 domain. For example, Lys197, Lys209, and Lys211 form salt bridges with the side chain of Asp652, and Lys213 forms a salt bridge with the phosphoryl oxygens of Ser657 (Fig. 5 *d*). Two phenylalanine residues of the HM, 653 and 656, are involved in ring-stacking interactions with the aromatic residues of C2: Tyr195, Trp245, and Trp247 (Fig. 5 *c*). The cation-π interactions between Lys197, Arg252, and the aromatic ring of Phe653 additionally stabilize the interface. All residues listed in Table S7, with the exception of Asn206, are conserved among the conventional PKCs.

Mutations at the C2-V5 interface affect PKCα conformation

To assess how the perturbation of the C2-V5 interface influences the conformational preferences of the enzyme, we made use of the intra-molecular steady-state FRET measurements. In the absence of full-length PKC structure, the relative placement of fluorophores in the auto-inhibited form is unclear, and the magnitude of FRET efficiency changes cannot be simply interpreted as the extent of conformational destabilization. We therefore used in vitro FRET results as a qualitative indication of the conformational perturbation.

Guided by the structural information about the C2•$(Ca^{2+})_2$•pHM complex, we designed mutations that target electrostatic and aromatic interactions and introduced them into mCer-PKCα-mCit-FLAG PKCα (see Figs. 5 and 6 *a*). Steady-state FRET experiments were conducted in the absence of PKC activators. Representative fluorescence spectra of PKCα variants illustrate the magnitude of FRET response (Fig. 6 *b*). The "no-FRET" control spectrum (*black trace*) was collected for the wild-type protein that was subjected to partial proteolysis that left mCit and mCer intact. In the spectrum of the intact wild-type PKCα (*blue trace*), the intensity of the mCit emission peak at 525 nm increases due to FRET between the protein termini. The fluorescence spectra of the PKCα variants illustrate the decrease in FRET efficiency due to perturbations of electrostatic and aromatic interactions at the interface.

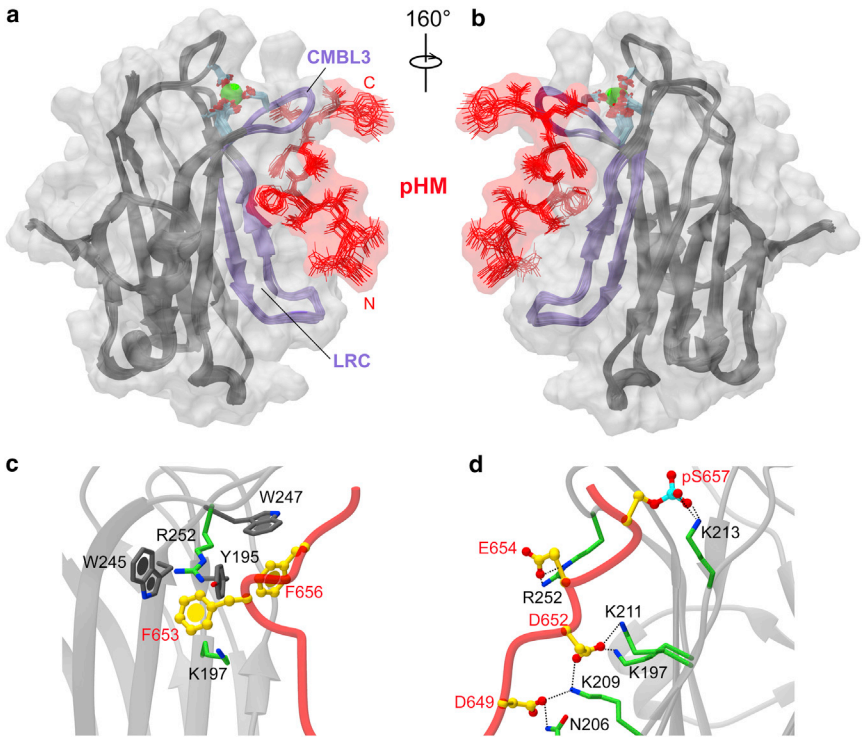

FIGURE 5 The C2-pHM interface is stabilized by electrostatic and aromatic interactions. (*a* and *b*) Twenty top-ranking structures of the C2•$(Ca^{2+})_2$•pHM complex, with pHM and LRC/CMBL3 highlighted in red and purple, respectively. Ca^{2+} ions are represented as green spheres. (*c* and *d*) The interface of the complex is stabilized by aromatic (*c*) and electrostatic (*d*) interactions. The charged/polar and aromatic side chains of C2 are shown in green and dark gray, respectively; all pHM side chains are colored gold. The interacting residues are labeled in red (pHM) and black (C2). To see this figure in color, go online.

The FRET data, presented as acceptor/donor intensity ratios, are divided into three groups according to the type/specifics of the targeted interaction (Fig. 6 *c*). The lowest FRET ratios are observed in variants that carry the mutation of residue Asp652 of the V5 domain. According to our structural model (Fig. 5), Asp652 is involved in electrostatic interactions with the lysine residues of the LRC. Mutation of Lys209 and Lys211 to glutamates in the KK variant also resulted in a decrease of FRET efficiency. The simultaneous charge reversal in the DKK variant does not produce a "wild-type" FRET response, indicating that the wild-type conformation cannot be simply recovered by simultaneous charge reversal. The disruption of the S657A/K213A interaction, as well as aromatic contacts, produced FRET ratios in the range 0.86–0.94. Overall, all PKCα variants generated in this study have lower FRET efficiencies compared to the wild-type protein, indicating perturbations of the C2-V5 interface.

Externally added pHM activates PKCα

If the nature of the C2-V5 interactions is auto-inhibitory, externally added pHM peptide should partially activate PKC in the absence of C2 agonists, Ca^{2+} and phosphatidylserine. We therefore tested the activity of PKCα in vitro in the presence of pHM under three conditions: 1) non-activating; 2) with a potent C1 agonist, PDBu, but no Ca^{2+} or lipids; and 3) fully activating, with Ca^{2+} and endogenous C1 ligand diacylglycerol, the latter incorporated into phosphatidylserine-containing LUVs (Fig. 7). In the absence of Ca^{2+} and PtdSer, pHM activated PKCα ~3.6-fold compared to the basal level. Similar behavior was observed in the presence of the C1 activator PDBu, where addition of pHM resulted in an ~2.4-fold increase in activity. These findings are consistent with pHM partially relieving the auto-inhibition of the enzyme. Under fully activating conditions, pHM had a slight inhibitory effect on PKCα. Our interpretation is that pHM competes with the phosphatidylserine-containing LUVs for the LRC site of the C2 domain, and thereby interferes with PKCα binding to the membrane-embedded diacylglycerol, which is required for full activation. Activation of PKCα by the externally added pHM peptide in the absence of C2 agonists is consistent with an auto-inhibitory role of V5, and is in agreement with the results of a previous study demonstrating that co-expression of the isolated V5 domain and PKCα increases the sensitivity of the enzyme to diacylglycerol in live cells (19).

DISCUSSION

Tight control over the PKC response to second messengers is achieved through conformational transition between the auto-inhibited inactive cytosolic state and the membrane-associated active state. The atomic-level structure of the full-length inactive PKC remains elusive. There are several lines of evidence that the canonical auto-inhibitory interaction between the pseudo-substrate region and the kinase

a

Variant	C2 mutation	V5 mutation
WT		
S657A		S657A
K213A	K213A	
D652A		D652A
DS		D652A/S657A
KKRDS	K197A/K209A/R252A	D652A/S657A
D652K		D652K
KK	K209E/K211E	
DKK	K209E/K211E	D652K
YW	Y195A/W247A	
FYYW	Y195A/W247A	F656A/Y658A
F656A		F656A

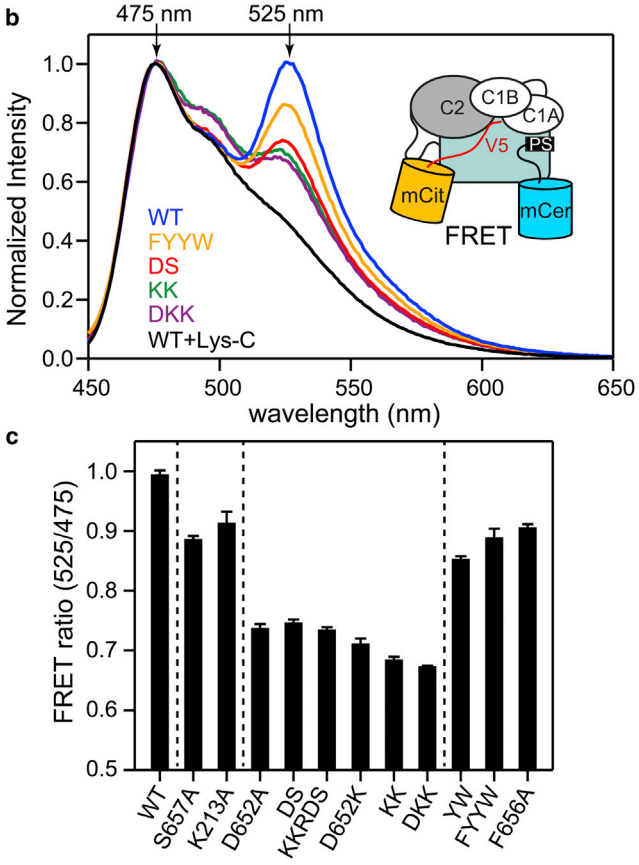

FIGURE 6 Mutations at the C2-V5 interface affect the conformation of PKCα. (*a*) Identity of PKCα variants. (*b*) Fluorescence emission spectra of the wild-type PKCα and selected variants. The schematic diagram depicts the PKCα construct used for in vitro fluorescence measurements. (*c*) FRET ratios (mean ± SE) of all variants obtained from at least three independent measurements. The grouping is the same as in (*a*). To see this figure in color, go online.

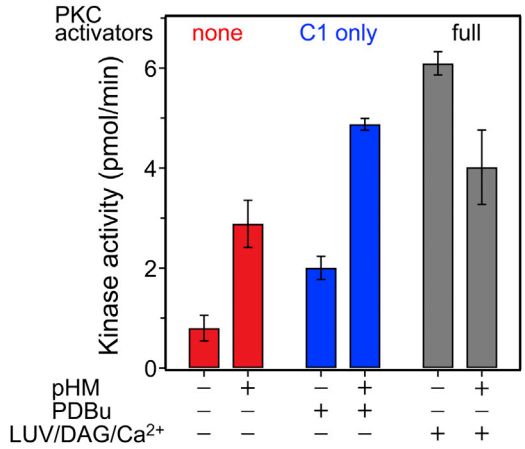

FIGURE 7 Externally added pHM activates PKCα in the absence of PKC agonists and in the presence of only the C1 agonist, PDBu. The activity data are shown as the mean ± SD. The data obtained with a full complement of effectors, Ca^{2+}, and LUVs comprising POPC/POPS/DAG 65:30:5 (mol %), are shown on the same plot for comparison. To see this figure in color, go online.

domain is augmented by other intra-molecular interactions in the inactive form (12,19,21,75,76). This work was motivated by two previous biochemical studies that explored the regulatory role of the HM of the C-terminal V5 region of PKC isoenzymes. Mutations in the HM region reduced the Ca^{2+} sensitivity of PKCβII (35) and increased the sensitivity of PKCα to diacylglycerol (19). Both findings suggested that there is an intra-molecular interaction between the C2 domain and HM that controls the sensitivity of PKC to its agonists.

Here, we present the structural model of the ternary complex between the C2 domain, Ca^{2+}, and the HM of the C-terminal V5 domain of PKCα (Fig. 5). The C2-V5 interface is formed by two highly conserved regions (Fig. 5 *a*), the LRC of the C2 domain and the HM, the latter being a general feature of the C-terminal domains in AGC kinases (77). In the crystal structures of α (26) and βII (27) catalytic domains, the phenylalanine residues of the HM interact with the hydrophobic pocket on the N-terminal lobe. The pSer residue is solvent exposed and anchored to the N-lobe by a hydrogen bond between its phosphoryl oxygens and the Nε2 hydrogens of Gln408 (α) and Gln411 (βII). The HM binding site on the C2 domain has similar features (Fig. 5, *c* and *d*). Three aromatic residues of C2, Tyr195, Trp245, and Trp247, provide a hydrophobic environment for the two phenylalanines of the HM, Phe653 and 656, resulting in the formation of the aromatic cluster at the C2-pHM interface. pSer657, Asp652, and Asp649 are involved in the electrostatic interactions with the lysine residues of the LRC region of C2.

Superposition of the C2•$(Ca^{2+})_2$•pHM and PtdIns(4,5)P_2-complexed C2 structures shows that the HM and PtdIns(4,5)P_2 occupy the same binding site, the LRC (Fig. 8 *a*). The role of PtdIns(4,5)P_2 in the context of PKC function is to augment the action of phosphatidylserine by decreasing the off-rate and thereby increasing the residency time of membrane-bound PKC (72,78). Moreover, since the cytosolic leaflet of the plasma membrane is selectively enriched with PtdIns(4,5)P_2, it may also play a role in targeting conventional PKCs to the plasma membrane. Our structural model suggests how the C2-V5 interaction may contribute to PKC localization. In the inactive enzyme, masking of

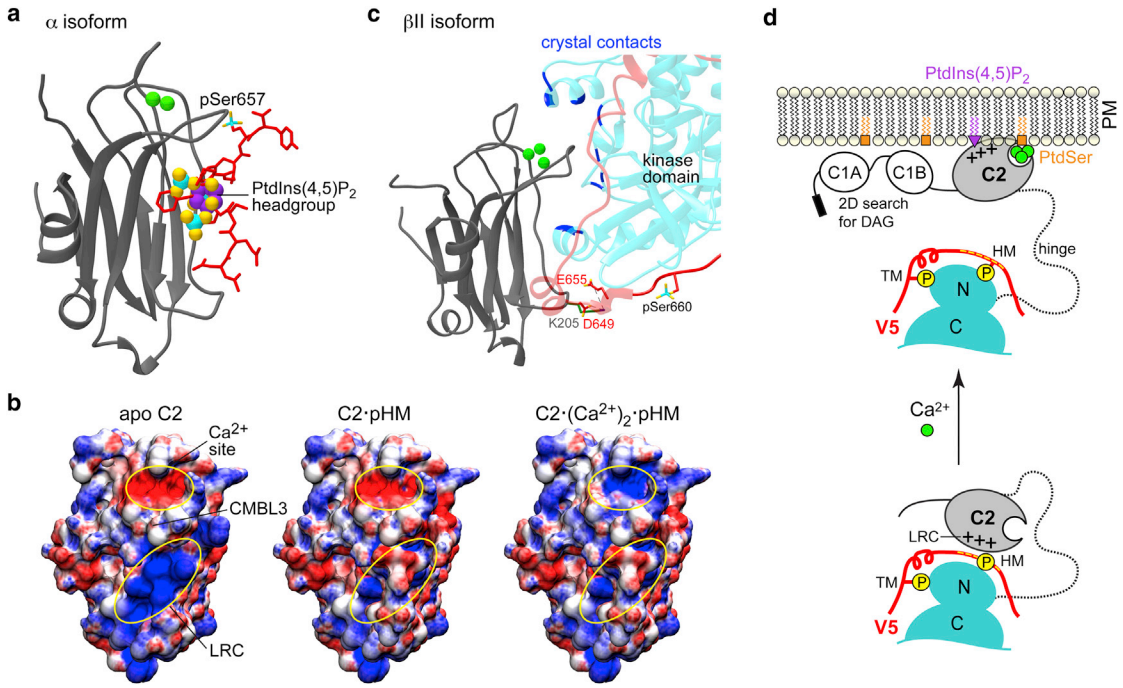

FIGURE 8 Proposed sensitizing and inhibitory roles of the C2-V5 interaction in PKCα. (*a*) Relative placement of the pHM and PtdIns(4,5)P_2 ligands, obtained from the backbone superposition of the C2 complexes: C2•$(Ca^{2+})_2$•pHM and PDB: 3GPE. The top-scoring C2•$(Ca^{2+})_2$•pHM structure is colored gray; the backbone representation of PDB: 3GPE is omitted for clarity. The headgroup of PtdIns(4,5)P_2 is shown in sphere representation. (*b*) Modulation of C2 electrostatic potential by Ca^{2+} and pHM. All electrostatic maps were calculated for apo C2, C2•pHM, and C2•$(Ca^{2+})_2$•pHM using the structure of the complex obtained in this work. The color coding corresponds to the electrostatic potential ranging from $-6k_bT/e$ (*red*) to $+6k_bT/e$ (*blue*). Binding of pHM to the LRC decreases the electrostatic potential of C2 and thereby increases its affinity to Ca^{2+}. (*c*) C2 domain crystal contacts in PKCβII (PDB: 3PFQ) that involve electrostatic interactions between C2 (K205) and V5 (E655 and D649). The relevance of this interaction for PKCβII auto-inhibition was established in a previous mutagenesis study (21). Other kinase residues that form an interface with the C2 domain are colored blue. (*d*) The proposed role of C2-V5 interactions in the first step of the PKCα activation process. To see this figure in color, go online.

the LRC by the C-terminal region would prevent C2 from fully interacting with the plasma membrane, until a high-affinity membrane-embedded ligand, such as PtdIns(4,5)P_2, is encountered. This interaction would then release C2 from the enzyme to the plasma membrane, thereby triggering the activation process, and allow V5 to form a full complement of interactions with the N-terminal lobe of the kinase.

The structural model of the C2•$(Ca^{2+})_2$•pHM complex also suggests a mechanism through which the C-terminal tail influences the Ca^{2+} sensitivity of PKC (35). Using the structure of the C2•$(Ca^{2+})_2$•pHM complex, we calculated the electrostatic potential maps for three states of C2: apo, C2•pHM, and C2•$(Ca^{2+})_2$•pHM (Fig. 8 *b*). The apo C2 shows two distinct areas, spatially separated by Ca^{2+}-binding loop 3, of the negative and positive potential corresponding to the metal ion-binding site and LRC, respectively. Binding of pHM masks the positively charged LRC and decreases the overall electrostatic potential of C2. This results in the increase of Ca^{2+} affinity to C2 that we observed in our binding experiments (Fig. 3 *b*). Destabilization of the C2-HM interface, e.g., through a mutation of the pSer residue (35), would impair the screening of the cationic LRC and decrease the Ca^{2+} affinity of the enzyme. The effect of the hydrophobic motif is therefore similar to that of PtdIns(4,5)P_2, which has been shown to increase the PKC affinity to Ca^{2+} (71,72,78) through modulation of the C2 electrostatic potential (70).

The interaction between the C2 and V5 domains is present in the partial crystal structure of PKCβII, PDB: 3PFQ (12). In what was originally identified as a crystal contact, the C2 domain clamps over the active site (Fig. 8 *c*); this conformation is stabilized by the interaction between Glu655 (the equivalent of D652 in α) and Lys205 of the LRC. The auto-inhibitory role of these interactions was established using mutagenesis and membrane translocation assays (21). Our model suggests a different arrangement of C2 and V5 in PKCα, where the hydrophobic motif masks the LRC, with pSer657 located next to the Ca^{2+}-binding loop 3. To visualize the C2 interaction with the C-terminal domain in the inactive kinase, we docked C2 onto the crystal structure of the inhibitor-complexed catalytic domain of PKCα that contains the C-terminal tail (26) (PDB: 3IW4, 2.8 Å resolution) using the NMR-derived restraints. The Ca^{2+}-binding regions of C2 are highly accessible to solvent in the top-scoring model (Fig. S10). We also note that the concentration of Ca^{2+} required for half-maximal activation of PKCα is 25-fold lower than that required for half-maximal activation of

PKCβII (79), possibly reflecting the enhanced accessibility of the C2 domain in the conformation adopted by PKCα.

In summary, our structural model provides a framework for understanding how the C-terminal V5 domain can influence the response of conventional PKCs to Ca^{2+} and contribute to their PtdIns(4,5)P_2 specificity (Fig. 8 *d*). The first step of conventional-PKC activation is the Ca^{2+}-dependent association of the C2 domain with anionic membranes. The pHM masks the positively charged LRC and thereby sensitizes the C2 domain to Ca^{2+} in the inactive closed form of the enzyme. At the plasma membrane, pHM is displaced from the LRC by high-affinity interaction of the latter with negatively charged phospholipids, such as PtdSer or PtdIns(4,5)P_2. This is followed by the diacylglycerol-driven membrane association of C1 domains, which ultimately leads to full enzyme activation.

CONCLUSIONS

Our data suggest that in the inactive cytosolic PKCα, the hydrophobic motif of V5 interacts with the LRC of the C2 domain. We propose that this interaction plays a dual regulatory role: 1) sensitization of PKCα to Ca^{2+} through screening of the LRC's positive charge and decreasing the overall electrostatic potential of C2; and 2) PKCα auto-inhibition, through masking the LRC until Ca^{2+}-complexed C2 encounters anionic lipids. This work illustrates the multifaceted role of the C-terminal domain in the regulation of PKCα activity. The ultimate goal of the structural biology studies of PKC is to obtain atomic-level information about all intra-molecular interactions that stabilize the inactive cytosolic state. This will potentially open up new routes for isoform-specific modulation of PKC activity, for both therapeutic and research purposes.

SUPPORTING MATERIAL

Supporting Materials and Methods, ten figures, and seven tables are available at http://www.biophysj.org/biophysj/supplemental/S0006-3495(17)35135-4.

AUTHOR CONTRIBUTIONS

T.I.I. conceived the research. Y.Y. conducted NMR experiments and in vitro activity measurements, as well as all relevant data analysis including structure calculation. C.S. and P.L. contributed reagents. T.I.I. wrote the article with input from Y.Y.

ACKNOWLEDGMENTS

This work was supported by Welch Foundation grant A-1784 (T.I.I.). Additional support was provided by National Institutes of Health grant GM108998 (T.I.I.) and National Science Foundation CAREER award CHE-1151435 (T.I.I.). Y.Y. was an American Heart Association predoctoral fellow (award no. 14PRE20380475).

REFERENCES

1. Nam, H. J., K. Boo, …, S. H. Baek. 2014. Phosphorylation of LSD1 by PKCα is crucial for circadian rhythmicity and phase resetting. *Mol. Cell.* 53:791–805.
2. Robles, M. S., C. Boyault, …, C. J. Weitz. 2010. Identification of RACK1 and protein kinase Cα as integral components of the mammalian circadian clock. *Science.* 327:463–466.
3. Rosse, C., M. Linch, …, P. J. Parker. 2010. PKC and the control of localized signal dynamics. *Nat. Rev. Mol. Cell Biol.* 11:103–112.
4. Poli, A., S. Mongiorgi, …, M. Y. Follo. 2014. Protein kinase C involvement in cell cycle modulation. *Biochem. Soc. Trans.* 42:1471–1476.
5. Reyland, M. E. 2007. Protein kinase C and apoptosis. *In* Apoptosis, Cell Signaling, and Human Diseases: Molecular Mechanisms. R. Srivastava, ed. Humana Press, pp. 31–55.
6. Castagna, M., Y. Takai, …, Y. Nishizuka. 1982. Direct activation of calcium-activated, phospholipid-dependent protein kinase by tumor-promoting phorbol esters. *J. Biol. Chem.* 257:7847–7851.
7. Antal, C. E., A. M. Hudson, …, A. C. Newton. 2015. Cancer-associated protein kinase C mutations reveal kinase's role as tumor suppressor. *Cell.* 160:489–502.
8. Mochly-Rosen, D., K. Das, and K. V. Grimes. 2012. Protein kinase C, an elusive therapeutic target? *Nat. Rev. Drug Discov.* 11:937–957.
9. Chen, L., H. Hahn, …, D. Mochly-Rosen. 2001. Opposing cardioprotective actions and parallel hypertrophic effects of δPKC and εPKC. *Proc. Natl. Acad. Sci. USA.* 98:11114–11119.
10. Hongpaisan, J., M. K. Sun, and D. L. Alkon. 2011. PKC ε activation prevents synaptic loss, Aβ elevation, and cognitive deficits in Alzheimer's disease transgenic mice. *J. Neurosci.* 31:630–643.
11. Igumenova, T. I. 2015. Dynamics and membrane interactions of protein kinase C. *Biochemistry.* 54:4953–4968.
12. Leonard, T. A., B. Różycki, …, J. H. Hurley. 2011. Crystal structure and allosteric activation of protein kinase C βII. *Cell.* 144:55–66.
13. Ziemba, B. P., J. Li, …, J. J. Falke. 2014. Single-molecule studies reveal a hidden key step in the activation mechanism of membrane-bound protein kinase C-α. *Biochemistry.* 53:1697–1713.
14. House, C., and B. E. Kemp. 1987. Protein kinase C contains a pseudosubstrate prototope in its regulatory domain. *Science.* 238:1726–1728.
15. Orr, J. W., and A. C. Newton. 1994. Intrapeptide regulation of protein kinase C. *J. Biol. Chem.* 269:8383–8387.
16. Steinberg, S. F. 2008. Structural basis of protein kinase C isoform function. *Physiol. Rev.* 88:1341–1378.
17. Cho, W., and R. V. Stahelin. 2006. Membrane binding and subcellular targeting of C2 domains. *Biochim. Biophys. Acta.* 1761:838–849.
18. Medkova, M., and W. Cho. 1998. Mutagenesis of the C2 domain of protein kinase C-α. Differential roles of Ca^{2+} ligands and membrane binding residues. *J. Biol. Chem.* 273:17544–17552.
19. Stensman, H., and C. Larsson. 2007. Identification of acidic amino acid residues in the protein kinase Cα V5 domain that contribute to its insensitivity to diacylglycerol. *J. Biol. Chem.* 282:28627–28638.
20. Stensman, H., A. Raghunath, and C. Larsson. 2004. Autophosphorylation suppresses whereas kinase inhibition augments the translocation of protein kinase Cα in response to diacylglycerol. *J. Biol. Chem.* 279:40576–40583.
21. Antal, C. E., J. A. Callender, …, A. C. Newton. 2015. Intramolecular C2 domain-mediated autoinhibition of protein kinase C βII. *Cell Reports.* 12:1252–1260.
22. Yang, Y., and T. I. Igumenova. 2013. The C-terminal V5 domain of Protein Kinase Cα is intrinsically disordered, with propensity to associate with a membrane mimetic. *PLoS One.* 8:e65699.
23. Xu, Z. B., D. Chaudhary, …, L. Mosyak. 2004. Catalytic domain crystal structure of protein kinase C-θ (PKCθ). *J. Biol. Chem.* 279:50401–50409.
24. Messerschmidt, A., S. Macieira, …, M. Blaesse. 2005. Crystal structure of the catalytic domain of human atypical protein kinase C-ι reveals

interaction mode of phosphorylation site in turn motif. *J. Mol. Biol.* 352:918–931.

25. Takimura, T., K. Kamata, …, Y. Iwasawa. 2010. Structures of the PKC-iota kinase domain in its ATP-bound and apo forms reveal defined structures of residues 533–551 in the C-terminal tail and their roles in ATP binding. *Acta Crystallogr. D Biol. Crystallogr.* 66:577–583.
26. Wagner, J., P. von Matt, …, S. Cottens. 2009. Discovery of 3-(1*H*-indol-3-yl)-4-[2-(4-methylpiperazin-1-yl)quinazolin-4-yl]pyrrole-2,5-dione (AEB071), a potent and selective inhibitor of protein kinase C isotypes. *J. Med. Chem.* 52:6193–6196.
27. Grodsky, N., Y. Li, …, S. Grant. 2006. Structure of the catalytic domain of human protein kinase C βII complexed with a bisindolylmaleimide inhibitor. *Biochemistry.* 45:13970–13981.
28. George, D. M., E. C. Breinlinger, …, J. J. Edmunds. 2015. Optimized protein kinase Cθ (PKCθ) inhibitors reveal only modest anti-inflammatory efficacy in a rodent model of arthritis. *J. Med. Chem.* 58:333–346.
29. George, D. M., E. C. Breinlinger, …, J. J. Edmunds. 2015. Discovery of selective and orally bioavailable protein kinase Cθ (PKCθ) inhibitors from a fragment hit. *J. Med. Chem.* 58:222–236.
30. Kjær, S., M. Linch, …, N. Q. McDonald. 2013. Adenosine-binding motif mimicry and cellular effects of a thieno[2,3-d]pyrimidine-based chemical inhibitor of atypical protein kinase C isoenzymes. *Biochem. J.* 451:329–342.
31. van Eis, M. J., J. P. Evenou, …, N. Soldermann. 2011. 2,6-Naphthyridines as potent and selective inhibitors of the novel protein kinase C isozymes. *Bioorg. Med. Chem. Lett.* 21:7367–7372.
32. Wang, C., Y. Shang, …, M. Zhang. 2012. Substrate recognition mechanism of atypical protein kinase Cs revealed by the structure of PKCι in complex with a substrate peptide from Par-3. *Structure.* 20:791–801.
33. Gao, T., A. Toker, and A. C. Newton. 2001. The carboxyl terminus of protein kinase c provides a switch to regulate its interaction with the phosphoinositide-dependent kinase, PDK-1. *J. Biol. Chem.* 276:19588–19596.
34. Newton, A. C. 2003. Regulation of the ABC kinases by phosphorylation: protein kinase C as a paradigm. *Biochem. J.* 370:361–371.
35. Edwards, A. S., and A. C. Newton. 1997. Phosphorylation at conserved carboxyl-terminal hydrophobic motif regulates the catalytic and regulatory domains of protein kinase C. *J. Biol. Chem.* 272:18382–18390.
36. Staudinger, J., J. Lu, and E. N. Olson. 1997. Specific interaction of the PDZ domain protein PICK1 with the COOH terminus of protein kinase C-α. *J. Biol. Chem.* 272:32019–32024.
37. Stebbins, E. G., and D. Mochly-Rosen. 2001. Binding specificity for RACK1 resides in the V5 region of βII protein kinase C. *J. Biol. Chem.* 276:29644–29650.
38. Abrahamsen, H., A. K. O'Neill, …, A. C. Newton. 2012. Peptidyl-prolyl isomerase Pin1 controls down-regulation of conventional protein kinase C isozymes. *J. Biol. Chem.* 287:13262–13278.
39. Morales, K. A., M. Lasagna, …, T. I. Igumenova. 2011. Pb^{2+} as modulator of protein-membrane interactions. *J. Am. Chem. Soc.* 133:10599–10611.
40. Rouser, G., S. Fkeischer, and A. Yamamoto. 1970. Two dimensional then layer chromatographic separation of polar lipids and determination of phospholipids by phosphorus analysis of spots. *Lipids.* 5:494–496.
41. Shaner, N. C., P. A. Steinbach, and R. Y. Tsien. 2005. A guide to choosing fluorescent proteins. *Nat. Methods.* 2:905–909.
42. Montaville, P., N. Coudevylle, …, S. Becker. 2008. The PIP2 binding mode of the C2 domains of rabphilin-3A. *Protein Sci.* 17:1025–1034.
43. Weiss, J. N. 1997. The Hill equation revisited: uses and misuses. *FASEB J.* 11:835–841.
44. Schmitz, C., M. J. Stanton-Cook, …, T. Huber. 2008. Numbat: an interactive software tool for fitting $\Delta\chi$-tensors to molecular coordinates using pseudocontact shifts. *J. Biomol. NMR.* 41:179–189.
45. Muhandiram, D. R., and L. E. Kay. 1994. Gradient-enhanced triple-resonance three-dimensional NMR experiments with improved sensitivity. *J. Magn. Reson. Ser B.* 103:203–216.
46. Clubb, R. T., V. Thanabal, and G. Wagner. 1992. A constant-time three-dimensional triple-resonance pulse scheme to correlate intraresidue ^{1}HN, ^{15}N, and ^{13}C′ chemical shifts in ^{15}N-^{13}C-labeled proteins. *J. Magn. Reson.* 97:213–217.
47. Grzesiek, S., J. Anglister, and A. Bax. 1993. Correlation of backbone amide and aliphatic side-chain resonances in 13C/15N-enriched proteins by isotropic mixing of ^{13}C magnetization. *J. Magn. Reson. B.* 101:114–119.
48. Montelione, G. T., B. A. Lyons, …, M. Tashiro. 1992. An efficient triple resonance experiment using carbon-13 isotropic mixing for determining sequence-specific resonance assignments of isotopically-enriched proteins. *J. Am. Chem. Soc.* 114:10974–10975.
49. Kay, L. E., G. Y. Xu, …, J. D. Formankay. 1993. A gradient-enhanced HCCH-TOCSY experiment for recording side-chain ^{1}H and ^{13}C correlations in H_2O samples of proteins. *J. Magn. Reson. Ser B.* 101:333–337.
50. Bax, A., G. M. Clore, …, L. E. Kay. 1990. Practical aspects of proton-carbon-carbon-proton three-dimensional correlation spectroscopy of ^{13}C-labeled proteins. *J. Magn. Reson.* 87:620–627.
51. Marion, D., P. C. Driscoll, …, G. M. Clore. 1989. Overcoming the overlap problem in the assignment of proton NMR spectra of larger proteins by use of three-dimensional heteronuclear proton-nitrogen-15 Hartmann-Hahn-multiple quantum coherence and nuclear Overhauser-multiple quantum coherence spectroscopy: application to interleukin 1.β. *Biochemistry.* 28:6150–6156.
52. Zuiderweg, E. R. P., and S. W. Fesik. 1989. Heteronuclear three-dimensional NMR spectroscopy of the inflammatory protein C5a. *Biochemistry.* 28:2387–2391.
53. Marion, D., L. E. Kay, …, A. Bax. 1989. Three-dimensional heteronuclear NMR of nitrogen-15 labeled proteins. *J. Am. Chem. Soc.* 111:1515–1517.
54. Zwahlen, C., P. Legault, …, L. E. Kay. 1997. Methods for measurement of intermolecular NOEs by multinuclear NMR spectroscopy: application to a bacteriophage lambda N-peptide/boxB RNA complex. *J. Am. Chem. Soc.* 119:6711–6721.
55. Iwahara, J., J. M. Wojciak, and R. T. Clubb. 2001. Improved NMR spectra of a protein-DNA complex through rational mutagenesis and the application of a sensitivity optimized isotope-filtered NOESY experiment. *J. Biomol. NMR.* 19:231–241.
56. Delaglio, F., S. Grzesiek, …, A. Bax. 1995. NMRPipe: a multidimensional spectral processing system based on UNIX pipes. *J. Biomol. NMR.* 6:277–293.
57. Goddard, T. D., and D. G. Kneller. 2008. SPARKY 3. University of California, San Francisco, CA.
58. Rieping, W., M. Habeck, …, M. Nilges. 2007. ARIA2: automated NOE assignment and data integration in NMR structure calculation. *Bioinformatics.* 23:381–382.
59. Shen, Y., F. Delaglio, …, A. Bax. 2009. TALOS+: a hybrid method for predicting protein backbone torsion angles from NMR chemical shifts. *J. Biomol. NMR.* 44:213–223.
60. Laskowski, R. A., J. A. Rullmannn, …, J. M. Thornton. 1996. AQUA and PROCHECK-NMR: programs for checking the quality of protein structures solved by NMR. *J. Biomol. NMR.* 8:477–486.
61. de Vries, S. J., A. D. J. van Dijk, …, A. M. Bonvin. 2007. HADDOCK versus HADDOCK: new features and performance of HADDOCK2.0 on the CAPRI targets. *Proteins.* 69:726–733.
62. Dominguez, C., R. Boelens, and A. M. Bonvin. 2003. HADDOCK: a protein-protein docking approach based on biochemical or biophysical information. *J. Am. Chem. Soc.* 125:1731–1737.
63. Hubbard, S. J., and J. M. Thornton. 1993. NACCESS computer program. Department of Biochemistry and Molecular Biology, University College London.
64. Daura, X., K. Gademann, …, A. E. Mark. 1999. Peptide folding: When simulation meets experiment. *Angew. Chem. Int.* 38:236–240.

65. Baker, N. A., D. Sept, …, J. A. McCammon. 2001. Electrostatics of nanosystems: application to microtubules and the ribosome. *Proc. Natl. Acad. Sci. USA.* 98:10037–10041.

66. Humphrey, W., A. Dalke, and K. Schulten. 1996. VMD: visual molecular dynamics. *J. Mol. Graph.* 14:33–38, 27–28.

67. Dolinsky, T. J., P. Czodrowski, …, N. A. Baker. 2007. PDB2PQR: expanding and upgrading automated preparation of biomolecular structures for molecular simulations. *Nucleic Acids Res.* 35:W522–W525.

68. Morales, K. A., Y. Yang, …, T. I. Igumenova. 2016. Dynamic response of the C2 domain of protein kinase Cα to Ca^{2+} binding. *Biophys. J.* 111:1655–1667.

69. Guerrero-Valero, M., C. Ferrer-Orta, …, S. Corbalán-García. 2009. Structural and mechanistic insights into the association of PKCα-C2 domain to PtdIns(4,5)P2. *Proc. Natl. Acad. Sci. USA.* 106:6603–6607.

70. Morales, K. A., and T. I. Igumenova. 2012. Synergistic effect of Pb^{2+} and phosphatidylinositol 4,5-bisphosphate on C2 domain-membrane interactions. *Biochemistry.* 51:3349–3360.

71. Guerrero-Valero, M., C. Marín-Vicente, …, S. Corbalán-García. 2007. The C2 domains of classical PKCs are specific PtdIns(4,5)P2-sensing domains with different affinities for membrane binding. *J. Mol. Biol.* 371:608–621.

72. Corbin, J. A., J. H. Evans, …, J. J. Falke. 2007. Mechanism of specific membrane targeting by C2 domains: localized pools of target lipids enhance Ca^{2+} affinity. *Biochemistry.* 46:4322–4336.

73. Verdaguer, N., S. Corbalan-Garcia, …, J. C. Gómez-Fernández. 1999. Ca^{2+} bridges the C2 membrane-binding domain of protein kinase Cα directly to phosphatidylserine. *EMBO J.* 18:6329–6338.

74. London, N., D. Movshovitz-Attias, and O. Schueler-Furman. 2010. The structural basis of peptide-protein binding strategies. *Structure.* 18:188–199.

75. Slater, S. J., J. L. Seiz, …, C. D. Stubbs. 2002. Regulation of PKCα activity by C1-C2 domain interactions. *J. Biol. Chem.* 277:15277–15285.

76. Stahelin, R. V., J. Wang, …, W. Cho. 2005. The origin of C1A-C2 interdomain interactions in protein kinase Cα. *J. Biol. Chem.* 280:36452–36463.

77. Pearce, L. R., D. Komander, and D. R. Alessi. 2010. The nuts and bolts of AGC protein kinases. *Nat. Rev. Mol. Cell Biol.* 11:9–22.

78. Manna, D., N. Bhardwaj, …, W. Cho. 2008. Differential roles of phosphatidylserine, PtdIns(4,5)P2, and PtdIns(3,4,5)P3 in plasma membrane targeting of C2 domains. Molecular dynamics simulation, membrane binding, and cell translocation studies of the PKCα C2 domain. *J. Biol. Chem.* 283:26047–26058.

79. Keranen, L. M., and A. C. Newton. 1997. Ca^{2+} differentially regulates conventional protein kinase Cs′ membrane interaction and activation. *J. Biol. Chem.* 272:25959–25967.